TU Delft

Delft University of Technology

The effect of hydrodynamics on the crystal nucleation of nearly hard spheres

Fiorucci, Giulia; Coli, Gabriele M.; Padding, Johan T.; Dijkstra, Marjolein

DOI
10.1063/1.5137815

Publication date
2020

Document Version
Final published version

Published in
Journal of Chemical Physics

Citation (APA)
Fiorucci, G., Coli, G. M., Padding, J. T., & Dijkstra, M. (2020). The effect of hydrodynamics on the crystal nucleation of nearly hard spheres. *Journal of Chemical Physics*, *152*(6), Article 064903. https://doi.org/10.1063/1.5137815

Important note
To cite this publication, please use the final published version (if applicable).
Please check the document version above.

Copyright
Other than for strictly personal use, it is not permitted to download, forward or distribute the text or part of it, without the consent of the author(s) and/or copyright holder(s), unless the work is under an open content license such as Creative Commons.

Takedown policy
Please contact us and provide details if you believe this document breaches copyrights.
We will remove access to the work immediately and investigate your claim.

This work is downloaded from Delft University of Technology.
For technical reasons the number of authors shown on this cover page is limited to a maximum of 10.

The Journal of Chemical Physics

The effect of hydrodynamics on the crystal nucleation of nearly hard spheres

Cite as: J. Chem. Phys. **152**, 064903 (2020); https://doi.org/10.1063/1.5137815
Submitted: 13 November 2019 . Accepted: 22 January 2020 . Published Online: 10 February 2020

Giulia Fiorucci, Gabriele M. Coli, Johan T. Padding, and Marjolein Dijkstra

View Online Export Citation CrossMark

ARTICLES YOU MAY BE INTERESTED IN

Studying rare events using forward-flux sampling: Recent breakthroughs and future outlook
The Journal of Chemical Physics **152**, 060901 (2020); https://doi.org/10.1063/1.5127780

Entire crystallization process of Lennard-Jones liquids: A large-scale molecular dynamics study
The Journal of Chemical Physics **152**, 054903 (2020); https://doi.org/10.1063/1.5139574

How does stiffness of polymer chains affect their adsorption transition?
The Journal of Chemical Physics **152**, 064901 (2020); https://doi.org/10.1063/1.5139940

Lock-in Amplifiers
Find out more today

Zurich Instruments

© 2020 Author(s).

The Journal of Chemical Physics ARTICLE scitation.org/journal/jcp

The effect of hydrodynamics on the crystal nucleation of nearly hard spheres

Cite as: J. Chem. Phys. 152, 064903 (2020); doi: 10.1063/1.5137815
Submitted: 13 November 2019 • Accepted: 22 January 2020 •
Published Online: 10 February 2020

View Online Export Citation CrossMark

Giulia Fiorucci,[1,a)] Gabriele M. Coli,[1] Johan T. Padding,[2] and Marjolein Dijkstra[1]

AFFILIATIONS

[1]Soft Condensed Matter, Debye Institute for Nanomaterials Science, Department of Physics, Utrecht University, Princetonplein 1, 3584 CC Utrecht, The Netherlands
[2]Process and Energy Department, TU Delft, Leeghwaterstraat 39, 2628 CB Delft, The Netherlands

[a)]**Author to whom correspondence should be addressed:** giulia.fiorucci7@gmail.com

ABSTRACT

We investigate the effect of hydrodynamic interactions (HIs) on the crystal nucleation of hard-sphere colloids for varying supersaturations. We use molecular dynamics and stochastic rotation dynamics techniques to account for the HIs. For high supersaturation values, we perform brute force simulations and compute the nucleation rate, obtaining good agreement with previous studies where HIs were neglected. In order to access low supersaturation values, we use a seeding approach method and perform simulations with and without HIs. We compute the nucleation rates for the two cases and surprisingly find good agreement between them. The nucleation rate in both cases follows the trend of the previous numerical results, thereby corroborating the discrepancy between experiments and simulations. Furthermore, we investigate the amount of fivefold symmetric clusters (FSCs) in a supersaturated fluid under different physical conditions, following the idea that FSCs compete against nucleation. To this end, we explore the role of the softness of the pair interactions, different solvent viscosities, and different sedimentation rates in simulations that include HIs. We do not find significant variations in the amount of FSCs, which might reflect the irrelevance of these three features on the nucleation process.

Published under license by AIP Publishing. https://doi.org/10.1063/1.5137815

I. INTRODUCTION

Homogeneous crystal nucleation of colloidal hard spheres has been the subject of many studies in the past 70 years. The first simulations were performed in the 1950s,[1,2] while the first experimental results were obtained in the 1980s.[3,4] The considerable body of work performed so far indicates the relevance of the topic both in fundamental physics and other disciplines.[5–10] Despite this, the mechanism by which a supersaturated fluid of colloidal hard spheres transforms into a crystal is still unclear. Several scenarios such as a one-step, two-step, devitrification, or spinodal-like process have been proposed,[11–15] but consensus has not yet been reached.

A simple theoretical framework for nucleation is known as the classical nucleation theory (CNT).[11,16,17] This theory describes homogeneous nucleation as a single-step process, where a crystal nucleus forms out of the metastable fluid and its probability to grow depends only on its size. However, recent investigations show that crystallization may also occur in two steps.[12–14] First, thermal fluctuations in the fluid cause the formation of preordered regions, known as precursors, and second, the precursors promote the formation of the actual crystal nucleus. The nature of the order in these precursors is still debated. Part of the scientific community believes that density fluctuations in the supersaturated fluid lead to local denser amorphous regions.[18,19] Others, instead, believe that bond-orientational order fluctuations lead to the formation of orientationally ordered structures.[15,20–22]

Another controversial topic concerns the rate of crystal nucleation. Several studies performed with different approaches and from different perspectives have tried to bridge the 20 orders of magnitude difference on the nucleation rate between experiments and simulations.[23–27] Despite the effort, it is still unclear why simulations display a much lower nucleation rate as compared to the experimental results. Several hypotheses have been proposed, but none of them conclusively prove what causes such a huge discrepancy.

For instance, in experiments, sterically stabilized polymethyl methacrylate (PMMA) particles in low polar solvent are considered

Published under license by AIP Publishing

to interact like hard spheres. The effect of residual charges or steric stabilizers on colloidal surfaces might, however, render their interaction slightly softer.[28] Therefore, it has been questioned whether the softness of the interaction potentially might be the missing ingredient in numerical models to recover the experimental nucleation rates. A numerical investigation initiated by Kawasaki and Tanaka[29] and followed by Filion *et al.*[30] and Richard and Speck,[31,32] has looked into this issue by simulating nearly hard particles interacting through the Weeks–Chandler–Andersen (WCA) potential.[33] The nucleation rate of this softer system is in good agreement with the earlier numerical results for hard spheres,[25,27] thus proving that introducing a small amount of softness does not influence the nucleation rate.

Another ingredient that is usually missing in simulation models concerns hydrodynamic interactions (HIs) among colloids. HIs do not affect the thermodynamic properties of the system, yet they have an influence on the particle dynamics and, hence, they might affect the nucleation process. HIs cannot be simplified to pairwise interactions due to their many-body character, hence their implementation requires the use of specific computationally expensive algorithms. Radu and Schilling[34] have included far-field HIs in their model system and have investigated the nucleation rate of hard spheres at different solvent viscosities. They remarkably find that a higher solvent viscosity leads to a higher nucleation rate; moreover, they predict larger effects for lower supersaturation. However, in their implementation, the near-field hydrodynamic interactions are neglected, and their work is limited to high supersaturation values where the fluid is characterized by a volume fraction of $\phi > 0.537$. The latter is due to limitations in computational time, which prevents one to directly probe the role of solvent viscosity at lower supersaturation where the numerical and experimental results start to deviate. Differently, Roehm *et al.*[35] found that HIs slow down the crystal growth in a system of soft colloids by using both Langevin dynamics and the fluctuating lattice Boltzmann method in order to include HIs in their model system.

Gravity also plays a non-negligible role in experiments. The solvent mixture is density matched to colloids in order to minimize the effect of gravity. Despite this, it is difficult to obtain an exact density matching, and some gravitational effects will remain present. Reference 36 showed that the literature on the experimental nucleation rates can be separated into two branches of slow and quick nucleation, corresponding to weak and strong sedimentation regimes, respectively. The hypothesis that gravity might enhance the nucleation rate has inspired both simulations and experiments to quantitatively measure this effect by intentionally introducing small gravitational effects in the system. Experiments by Ketzetzi *et al.*[37] display a strong enhancement of the nucleation rate due to gravity. The results also indicate that such enhancement is caused by collective hydrodynamic effects during sedimentation rather than by changes in the local volume fraction. The numerical study by Russo *et al.*,[38] where HIs are neglected, also shows higher nucleation rates under sedimentation. The enhancement is attributed here to the formation of an inhomogeneous density profile, where crystal nuclei are more likely to form in the fluid at a local volume fraction of $\phi \sim 0.56$.

Another research branch has recently focused on analyzing the local structure of supersaturated fluids and, particularly, on the detection of fivefold symmetric clusters (FSCs). This interest originates from previous studies which highlight that fivefold symmetric clusters can suppress crystallization in supercooled fluids, eventually leading to vitrification.[39,40] In analogy with hard spheres at high supersaturation, the presence of fivefold local arrangements might inhibit the nucleation process.

A recent numerical study has shed light on the mechanism by which these clusters compete with nucleation.[41] They implemented a model system where the amount of pentagonal bipyramids can be tuned and showed that the presence of such clusters has an influence on both the thermodynamic and kinetic aspects of nucleation. In particular, the authors found that the fluid–solid coexistence boundaries shift toward lower volume fractions (thermodynamic aspect) and that the nucleation rate increases (kinetic aspect) by decreasing the amount of pentagonal bipyramids. This study has revealed the nucleation process from a different perspective and suggests an alternative approach to the problem. However, this investigation is not concerned with understanding which physical conditions promote or suppress the formation of fivefold symmetric clusters in the fluid.

A recent study by Wood *et al.*[36] made progress in this direction. It showed that the amount of defective icosahedral clusters decreases considerably by increasing gravity. With these preliminary but encouraging results, they also studied the nucleation rate of the fluid under the effect of gravity by using the simulation model[41] described above. The amount of fivefold clusters measured in the sedimenting fluid in experiments has been mapped to the amount of clusters in the simulated fluid. This study predicted a nucleation rate of five orders of magnitude larger than the nucleation rate of a gravity-free fluid.[36] This is in agreement with expectations set by the fivefold picture, but unfortunately the enhancement is not enough to explain the high nucleation rates in experiments in the weak sedimentation regime.[36]

In the present work, we study crystal nucleation of nearly hard spheres with different numerical methods, all including (far-field and near-field) HIs in our model system. In Sec. III, we compute the nucleation rate by direct observation of crystal nuclei forming out of a homogeneous supersaturated fluid. As the required computational time increases rapidly upon lowering the supersaturation, this investigation is limited to high supersaturation. To overcome this problem and have access to lower supersaturation, we use a seeding approach method[42,43] in Sec. IV. Here, we compare the nucleation rate obtained in a model system which includes HIs, to one where HIs are neglected. Finally, in Sec. V, we further investigate different physical conditions that may affect the local structure of the fluid phase, particularly, the presence of fivefold symmetric clusters. In particular, we retrace the hypothesis mentioned above and investigate the role of softness of the particle interactions, different solvent viscosities, and gravitational effects, in the local structure of a low supersaturated fluid phase.

II. MODEL AND METHODS

A. The model system

We consider a system of N colloidal spheres with a diameter σ in a volume V, interacting via the Weeks–Chandler–Andersen (WCA) pair potential.[33] Two colloids at a relative center-to-center distance r experience a repulsion of the form

Published under license by AIP Publishing

$$\beta U(r) = \begin{cases} 4\beta\varepsilon\left[\left(\frac{\sigma}{r}\right)^{12} - \left(\frac{\sigma}{r}\right)^{6} + \frac{1}{4}\right] & r \le 2^{1/6}\sigma, \\ 0 & r > 2^{1/6}\sigma, \end{cases} \quad (1)$$

where ε is the energy scale and $\beta = 1/k_B T$ with k_B being the Boltzmann constant and T being the temperature. If not stated otherwise, we consider a repulsion strength of $\beta\varepsilon = 40$. The freezing density of this system is known from the literature, $\rho_f \sigma^3 = 0.712$,[30] with $\rho = N/V$ being the density. In order to map this system onto hard spheres, we equate the freezing volume fraction of hard spheres $\phi_f^{HS} = 0.492$ to the freezing volume fraction of our system $\phi_f = \pi\rho_f\sigma_{eff}^3/6$, with σ_{eff} being the effective diameter of the colloids, and find $\sigma_{eff} = 1.097\sigma$. Hence, we define the volume fraction as $\phi = \pi\rho\sigma_{eff}^3/6$, which directly compares with the volume fraction of hard spheres.

We perform simulations in the canonical ensemble using the Large-scale Atomic/Molecular Massively Parallel Simulator (LAMMPS)[44,45] software, by using molecular dynamics (MD) in combination with the stochastic rotation dynamics (SRD) technique. The hydrodynamic effects are rendered by the presence of point particles, which we call SRD particles. They represent a coarse-graining of the solvent molecules over space and time. Physical properties of the solvent are extracted from space and time averages.[46]

The SRD algorithm consists of two steps, the streaming and the collision step. During the streaming step, SRD particles behave like an ideal gas among themselves, but they exchange momentum with the colloids via hard collisions. A colloid and an SRD particle collide at a relative distance $r' = 0.465\sigma$, which is slightly smaller than the colloid radius of 0.5σ. This guarantees that the SRD particles are isotropically distributed around the colloid surface, in order to prevent spurious depletion effects between the colloids.[47] In fact, two colloids at a relative distance $2r' = 0.93\sigma$ experience a repulsion of $\beta U(2r') \simeq 175$, which makes the occurrence of two colloids at a distance $r < 0.93\sigma$ extremely unlikely. We employ the slip boundary condition on the colloid surface.

Every time interval $\Delta t_c = 4\tau_{MD}$, where τ_{MD} is the molecular dynamics integration time step, SRD particles exchange momentum among themselves via the stochastic rotation dynamics algorithm, and their velocities are rescaled in order to keep the temperature fixed in the system. We implement the Galilean-invariant thermostat of Hecht *et al.*[48] Colloidal particles are, therefore, thermalized by collisions with SRD particles, which act as a thermal bath.

The SRD fluid is characterized by a mean free path $\lambda = 0.023\sigma$ and a number density $\gamma = 5/a_0^3$, where $a_0 \simeq 0.23\sigma$ is the SRD grid cell. We compute the solvent shear viscosity η by using the expression reported in Refs. 48–50 and obtain $\eta = m_f[\gamma a_0^3 - 1 + \exp(-\gamma a_0^3)]/(18\Delta t_c a_0) + k_B T\gamma\Delta t_c(\gamma a_0^3 + 2)/[4(\gamma a_0^3 - 1)] = 3.51\,\eta_0$, where $\eta_0 = \sqrt{M_c k_B T}/\sigma^2$ is expressed in colloid mass units M_c and m_f is the mass of an SRD particle.

We note that the SRD fluid is more compressible than a molecular solvent. However, with a proper separation of time scales between that of the solvent and that of the colloids, the solvent can be viewed as effectively incompressible; if the diffusivity of the SRD fluid particles is much larger than that of the colloids, the density variations are relatively small. This was also confirmed in the work of Theers *et al.*[51] for actively moving colloids known as squirmers. In their Appendix C, Theers *et al.* showed that for sufficiently low activity of the squirmers (low pumping number), the SRD density variations are small.

In Sec. V, we investigate whether the variation of some system properties has any influence on the local structure of the fluid, in particular, on the formation or suppression of fivefold symmetric clusters (FSCs). In order to do so, we vary some of the parameter values described above. We explore the effect of softness of the colloid interactions by varying the temperature $\beta\varepsilon = 40$, 10, and 5, which in turn changes the size of the effective colloid diameter. In order to map the softer system onto the hard-sphere system, we compute the effective diameter by performing free energy calculations and computing the freezing density. For $\beta\varepsilon = 10$ and $\beta\varepsilon = 5$, we obtain $\sigma_{eff} = 1.072\sigma$ and $\sigma_{eff} = 1.056\sigma$, respectively. We compare our values with the literature and find good agreement with those in the work of Ahmed and Sadus,[52] which found $\sigma_{eff} = 1.073\sigma$ and $\sigma_{eff} = 1.055\sigma$ for $\beta\varepsilon = 10$ and $\beta\varepsilon = 5$, respectively. Further details on free energy calculations are provided in Sec. II B.

We investigate the role of solvent viscosity by varying the number density of SRD particles in the range $5 \le \gamma a_0^3 \le 200$, corresponding to a solvent viscosity of $3 \lesssim \eta/\eta_0 \lesssim 165$.

Finally, we investigate the system in a gravitational field. To do so, we impose an external force F_{col} on each colloid, pointing to the negative z-direction. We also reproduce the effect of back-flow in the solvent by imposing a force f_{srd} on each SRD particle, which points to the positive direction of z. The force acting on N colloids $N \times F_{col}$ is balanced by the force acting on N_f SRD particles $N_f \times f_{srd}$, leading to conservation of the center of mass velocity, which was initially imposed to be zero. We perform simulations at Péclet number $Pe = 0$, 0.5, 1.0, 1.5, and 2.0, where $Pe = v\sigma_{eff}/2D_0$ is the ratio of advection over diffusion. Here, v and D_0 are, respectively, the terminal velocity and diffusion coefficient of the colloidal particles in the limit of very low volume fraction ($\phi \sim 0.001$). In all simulations, we use periodic boundary conditions in all three directions (x, y, and z), and the system size ranges from 4000 to 7000 colloidal particles, with an order of 2×10^6 solvent particles.

B. Free energy calculations

The fluid and fcc coexistence densities of the WCA systems are calculated by determining the free energies of both phases, in combination with a common-tangent construction. The Helmholtz free energy per particle $f = F/N$, as a function of density ρ is calculated using thermodynamic integration of the equations of state,[53]

$$\beta f(\rho) = \beta f(\rho_0) + \int_{\rho_0}^{\rho} d\rho' \frac{\beta P(\rho')}{\rho'^2}, \quad (2)$$

where $\rho = N/V$ is the density with N being the number of particles and V being the volume of the system, $f(\rho_0)$ denotes the Helmholtz free energy per particle for the reference density ρ_0, $\beta = 1/k_B T$ is the inverse temperature, and P is the pressure. The equations of state for both phases are calculated using MC simulations in the NPT ensemble using $N = 1372$ particles. Concerning the fluid phase, we use the ideal gas as a reference state.

Differently, for the fcc crystal, we employ the Frenkel–Ladd method to calculate the Helmholtz free energy at a reference density ρ_0 using MC simulations in the NVT ensemble.[54] We repeat the

Published under license by AIP Publishing

process for $N = 256$, 500, 864, and 1372 in order to take into account finite-size effects and extrapolate to an infinite system.[55] The reference densities employed for $\beta\varepsilon = 40$, 10, and 5 are, respectively, $\rho_0\sigma^3 = 0.81$, 0.85, and 0.89.

Subsequently, the fcc–fluid coexistence densities for different temperatures $\beta\varepsilon$ are calculated by employing a common-tangent construction on the fluid and fcc free energy density curves in the $\beta f - \frac{1}{\rho}$ plane.

C. Local structure analyses

In order to distinguish a crystal structure from the amorphous fluid on a single particle level, we use the bond-orientational order parameter.[56,57] This algorithm detects whether particle i belongs to a crystal or fluid environment based on the arrangement of its closest neighbors $N_b(i)$. The algorithm associates with each particle i a complex vector $q_{lm}(i)$ defined as

$$q_{lm}(i) = \frac{1}{N_b(i)} \sum_{j=1}^{N_b(i)} Y_{lm}(\mathbf{r}_{ij}), \tag{3}$$

where l is a free integer parameter, m is an integer defined in the range $-l \le m \le l$, and $Y_{lm}(\mathbf{r}_{ij})$ are the spherical harmonics. The sum runs over the nearest $N_b(i)$ neighbors of particle i and the vector $\mathbf{r}_{ij}$ connects particle i to particle j. We compute the scalar product of q_{lm} of neighboring particles i and j,

$$S_l(i,j) = \frac{\sum_{m=-l}^{l} q_{lm}(i) q_{lm}^*(j)}{\left(\sum_{m=-l}^{l} |q_{lm}(i)|^2\right)^{1/2} \left(\sum_{m=-l}^{l} |q_{lm}(j)|^2\right)^{1/2}}, \tag{4}$$

where the symbol * indicates the complex conjugate. We define i and j connected if $S_l(i, j) > d$, where d is a threshold parameter. Finally, particle i belongs to a crystal environment if it has a number of connections n_c larger than a threshold $n_c \ge c$. If this is the case, we label it solid-like, otherwise liquid-like. As a result, we are able to identify all the solid-like particles and perform a cluster analysis which assigns all the solid-like connected particles to a single cluster. Therefore, each solid-like particle belongs only to one cluster. Nearly hard-sphere particles form a crystal nucleus characterized by random hexagonal order and 12 nearest neighbors; therefore, we choose $l = 6$ and $N_b(i) = 12$. The thresholds $d = 0.7$ and $c = 7$ are optimized for the detection of solid-like particles in this system.[27,30]

We analyze the amount of fivefold symmetric clusters in the supersaturated fluid via the topological cluster classification (TCC) algorithm.[58] One parameter involved in the definition of a bond is f_c, which is set to 0.82, in line with the analyses performed by Wood *et al.*[36]

III. BRUTE FORCE SIMULATIONS

This simulation method enables us to calculate the nucleation rate of nearly hard-sphere colloids by directly observing the nucleation events originating from a supersaturated fluid. We perform MD + SRD simulations in order to account for HIs in our model. We simulate a system composed of $N = 4000$ colloids interacting with a WCA potential with $\beta\varepsilon = 40$ in different box volumes V, chosen such that the volume fraction of interest is acquired. We set the number density of SRD particles $\gamma a_0^3 = 5$ and the integration time step $\tau_{\mathrm{MD}} = 4.5 \times 10^{-4}\sigma\sqrt{M_c/(k_BT)}$, with SRD collision time $\Delta t_c = 4\tau_{\mathrm{MD}}$. These parameters are chosen such that the SRD fluid displays the properties of a viscous solvent in the Stokes limit, while maintaining a feasible computational time. We verify that SRD particles reproduce the dynamics of a solvent by computing the Schmidt number Sc, which compares the rate of diffusive momentum transfer relative to the rate of diffusive mass transfer in the solvent, and which is much greater than 1 for liquid-like systems. In our system, we have $\mathrm{Sc} \simeq 6$, which confirms a liquid-like dynamics. By using the aforementioned parameters, we obtain a colloid dynamics characterized by a self-diffusion constant $D_0 = 0.0573\sigma\sqrt{k_BT/M_c}$, which we measure from the mean squared displacement of a particle in a very dilute system ($\phi \simeq 0.001$). From the self-diffusion constant, we derive the Brownian time $\tau_B = \sigma^2/D_0$, which we use as the unit of time in this section. We generate an equilibrated initial configuration and ensure that the fraction of crystalline particles is below 1% at time $t = 0$ of the simulation run. During the simulation run, we monitor the crystallinity fraction ξ of the system, which is defined as the ratio of crystalline particles over the total number of particles. We define the nucleation time τ_n as the time that elapses until we obtain $\xi = 0.10$. Hence, the nucleation rate reads

$$\kappa = \frac{1}{\langle \tau_n \rangle V}, \tag{5}$$

where $\langle \tau_n \rangle$ is the nucleation time averaged over several simulation runs. We show the crystallinity fraction ξ as a function of the

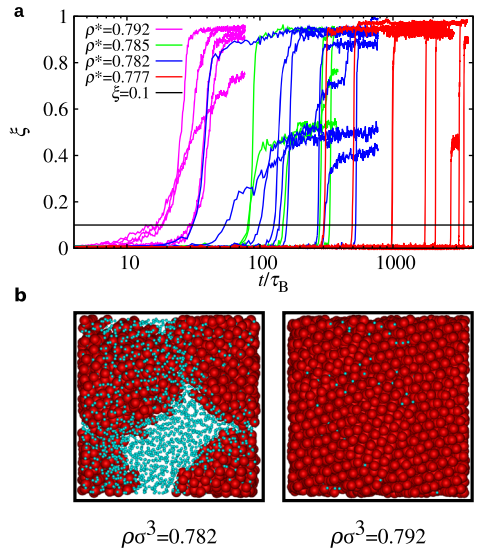

FIG. 1. (a) Fraction of crystalline particles as a function of time for different densities $\rho^* = \rho\sigma^3$, represented here by different colors. The curves of the same color are independent realizations performed at the same density. (b) Snapshots of the system taken after the nucleation event. (Left) Configuration of the system with $\rho\sigma^3 = 0.781\,53$, showing a fluid–crystal coexistence. The particles that belong to a crystal domain are colored red, and those belonging to a fluid phase are colored cyan and reduced in size to enhance the visualization. (Right) Configuration of the system with $\rho\sigma^3 = 0.792\,28$, showing a full crystallization.

Published under license by AIP Publishing

rescaled time t/τ_B in Fig. 1(a), where different colors indicate different fluid densities, while trajectories with the same color represent independent runs at the same density.

The sharpness of the transition from the fluid to the crystal phase guarantees that our criterion to define the nucleation time is reasonable. In fact, the largest source of error comes from the spread in nucleation times across different simulation runs, rather than the choice of the threshold. Note that the crystallinity fraction ξ reaches very high values ($\xi > 0.8$) in many simulation runs, but also saturates around $\xi \simeq 0.5$ in some other cases, where we observe a coexistence between the fluid and the crystal. As all the simulated densities, except for $\rho\sigma^3 = 0.792\,28$, fall in the fluid–solid coexistence region of the phase diagram, but closer to the melting density $\rho_M\sigma^3 = 0.784$[30] than the freezing density $\rho_F\sigma^3 = 0.712$,[30] we indeed expect high values for the crystallinity fraction $\xi > 0.9$. We believe that the systems are kinetically trapped for the states characterized by a lower ξ. This, however, does not influence our results on τ_n, which is determined by the time that the system reaches a crystallinity fraction $\xi = 0.10$. We display two configurations, well equilibrated after the nucleation event, in Fig. 1(b). The left panel shows a snapshot of the system with a density of $\rho\sigma^3 = 0.781\,53$, where the fluid coexists with the crystal phase and displays a crystallinity fraction of $\xi = 0.50$. We represent the crystalline and fluid particles in red and cyan, respectively. The fluid particles are reduced in size to enhance the visualization. In the right panel of Fig. 1(b), the system has a density of $\rho\sigma^3 = 0.792\,28$ and has (almost) fully crystallized ($\xi = 0.95$).

In Table I, we report the results of the average nucleation time $\langle\tau_n\rangle/\tau_B$ and the nucleation rate $\kappa\sigma_{\rm eff}^5/D_0$, together with the density of the fluid $\rho\sigma^3$, the number of simulations performed for each density n_{tr}, and the number of observed nucleation events n_e. In case there are less nucleation events than trials, we calculate the nucleation rate from Eq. (5) by considering a larger volume of the simulation box given by $V' = Vn_{tr}/n_e$.

In Fig. 2, we show the nucleation rate $\kappa\sigma_{\rm eff}^5/D_0$ as a function of the mapped volume fraction ϕ. Our results are represented by red squares, while the previous numerical and experimental results are shown in blue and green symbols, respectively.

We observe that our data points are in very good agreement with the literature, which we expected at these high packing fractions. Therefore, we conclude that HIs do not affect the nucleation rate at high supersaturations. Yet, we need to access lower fluid supersaturations in order to understand whether HIs play a role in the enhancement of the nucleation rate, as observed

TABLE I. Nucleation rates $\kappa\sigma^5/D_0$ of nearly hard spheres obtained from brute force simulations which include HIs. We perform n_{tr} simulations for each fluid density $\rho\sigma^3$ and report the number of simulations that have nucleated n_e and the average nucleation time $\langle\tau_n\rangle/\tau$.

$\rho\sigma^3$	n_{tr}	n_e	$\langle\tau_n\rangle/\tau_B$	$\kappa\sigma_{\rm eff}^5/D_0$
0.792 28	5	5	22.6	1.38×10^{-5}
0.785 07	5	5	185	1.68×10^{-6}
0.781 53	10	10	190	1.64×10^{-6}
0.777 00	20	10	1130	1.38×10^{-7}

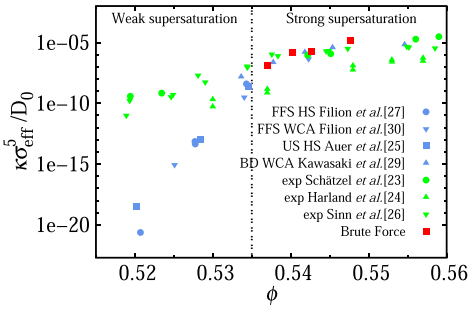

FIG. 2. Nucleation rate $\kappa\sigma_{\rm eff}^5/D_0$ as a function of the mapped volume fraction ϕ. Green symbols represent the experimental results, blue symbols are the numerical results obtained without accounting for HIs, and red squares represent our results, obtained with brute force simulations including HIs.

experimentally. In fact, the previous numerical results, obtained without HIs, differ from the experimental results by approximately two orders of magnitudes at a volume fraction of $\phi \simeq 0.535$, and the difference becomes even larger for lower volume fractions, in the range of weak supersaturation, as illustrated in Fig. 2. However, directly computing the nucleation rate in the region of weak supersaturation becomes impractical via brute force simulations. For instance, the experimental nucleation rate at $\phi = 0.53$ is at least one order of magnitude smaller as compared to the nucleation rate at $\phi = 0.535$. We obtain the results at $\phi = 0.537$ in a simulation time of about 2 months, thereby confirming that this method becomes inadequate at such low volume fractions. In Sec. IV, we overcome this problem by employing another simulation method.

IV. THE SEEDING APPROACH

In Sec. III, we provided the results on the nucleation rate of nearly hard spheres with HIs by performing brute force simulations. However, the use of this numerical approach at low supersaturation is hindered by the enormous computational time required to observe a nucleation event to occur. Several biasing techniques have been used to access volume fractions lower than 0.535, like umbrella sampling and forward flux sampling.[27,30,31] Recently, a new simulation technique has provided quite accurate results on both the thermodynamic and kinetic aspects of nucleation. This technique is known as the seeding approach,[42,43] and it has been applied to study the nucleation barrier of nearly hard spheres with $\beta\varepsilon = 40$.[32]

In this section, we aim to understand the relevance of HIs on the nucleation process of a colloidal fluid at low supersaturation. To do so, we employ a seeding approach method and implement both the MD and the MD + SRD techniques to neglect or account for HIs in the model system, respectively. We compute the nucleation rate for different nucleus sizes and compare the results obtained with the two simulation schemes.

The seeding approach is based on the classical nucleation theory and involves seeding the supersaturated fluid with a crystalline nucleus, and determining the thermodynamic conditions at which the nucleus is critical, i.e., it has equal probability to shrink or grow.

Published under license by AIP Publishing

We perform simulations in the *NVT* ensemble, with $\beta\varepsilon = 40$ for different densities. For each size of the nucleus, we determine the density at which the nucleus is critical and we refer to it as the critical density ρ_c.

In order to determine the critical density, we compute the probability of melting $P_m(\rho)$ determined by the fraction of trajectories that display a complete melt of the nucleus, leading to $n < 10$. In Fig. 3(a), we show ten independent trajectories of a nucleus of size n as a function of time. We obtained these realizations by performing simulations with HIs. The committor probability $P_c(\rho) = 1 - P_m(\rho)$ reflects the probability that the seed grows out and induces a fluid–solid phase transition in the system at fixed density ρ. We report the committor probability as a function of the density of the system in Fig. 3(b), displayed here with dots. We obtain these results for a seed of size $\langle n\rangle = 430 \pm 40$, in a system composed by $N = 7000$ particles and account for HIs. The seed is initially composed of $\langle n\rangle = 430 \pm 40$ particles, where the angular brackets indicate an average of the nucleus size performed over the first time interval $t/\tau_{MD} = 5 \times 10^4$ at the critical density ρ_c. We fit the function $P_c(\rho) = 1/2[1 + \mathrm{erf}(a(\rho - \rho_c))]$ on the numerical data, where a and ρ_c are fitting parameters. The fit is shown with a solid line, and it directly provides the critical density $\rho_c\sigma^3 = 0.751$ for this seed size, which corresponds to the density where $P_c = 1/2$.

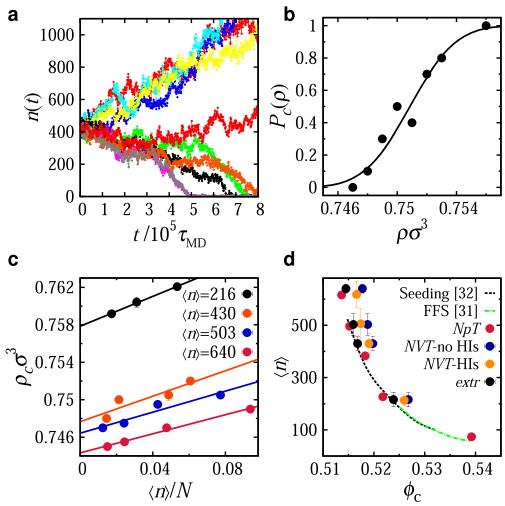

FIG. 3. The seeding approach. (a) Time evolution of a crystalline seed of 430 particles at temperature $k_BT = 0.025\ \varepsilon$ and critical density $\rho_c\sigma^3 = 0.751$ for 10 independent trajectories, using MD simulations with HIs. The total number of particles is 7000. (b) The committor probability as a function of density for a seed of 430 particles in a system of 7000 particles. The solid line represents the fit performed to obtain the critical density ρ_c at $P_B = 1/2$. (c) Critical density as a function of system size for different seeds, as obtained from MD simulations without HIs in the *NVT* ensemble. The solid line indicates the linear fit performed on the dataset to extrapolate the critical density to the thermodynamic limit at $\langle n\rangle/N = 0$. (d) Seed size as a function of the critical volume fraction $\phi_c = \pi\rho_c\sigma^3_{\mathrm{eff}}/6$. Data obtained from *NpT* simulations are not affected by finite-size effects, while data obtained from *NVT* simulations show a higher critical volume fraction. The black dots represent the values of the critical volume fraction obtained from the finite-size scaling study, reported in (c). The dashed black and dashed-dotted green lines are interpolations of the results reported in Refs. 31 and 32.

As mentioned earlier, we perform simulations in the *NVT* ensemble for which it is possible to implement HIs. In this ensemble, however, the stability of the seed is influenced by finite-size effects.[32] In fact, given a seed of size n, the critical density found with a system of N particles is higher as compared to the critical density we would obtain with an infinitely large system, which corresponds to the thermodynamic limit. This effect is due to the progressive depletion of colloidal particles in the supersaturated fluid phase which surround the nucleus, while the latter is increasing in size. As we increase the total system size N, this effect becomes less relevant and we detect a lower critical density. In Fig. 3(c), we report the results on the finite-size scaling, which are performed without including HIs, due to the huge computational cost that the MD + SRD method requires for large system sizes. We show the critical density ρ_c as a function of the system size $\langle n\rangle/N$ for four seed sizes $\langle n\rangle = 216$, 430, 503, and 640, here represented by points in different colors. We observe that ρ_c increases linearly with the inverse system size; therefore, we perform a linear fit to extrapolate the critical density ρ_c^{extr} in the thermodynamic limit at $\langle n\rangle/N = 0$.

In Fig. 3(d), we show the seed size $\langle n\rangle$ and its corresponding critical volume fraction $\phi_c = \pi\rho_c\sigma^3_{\mathrm{eff}}/6$, for simulations performed in different ensembles. The red points represent the results obtained from MD simulations in the *NpT* ensemble. In this ensemble, the growth of the seed is not affected by the system size, since the pressure of the fluid is constant over time. These points are in good agreement with the results obtained in Refs. 31 and 32, where they use both the seeding approach and forward flux sampling methods. For ease of comparison, we report here an interpolation of their results with dashed black and dashed-dotted green lines for the seeding and forward flux sampling methods, respectively. The orange and blue points are obtained from simulations on a finite system in the *NVT* ensemble, where hydrodynamic interactions are included and neglected, respectively. The system size varies in the range $0.053 < \langle n\rangle/N < 0.094$. In both cases, finite-size effects are present and determine a higher critical volume fraction as compared to *NpT* simulations.

Interestingly, we observe that the simulations in the *NVT* ensemble provide slightly different critical volume fractions for the two cases of including and neglecting HIs. This difference is not significantly large, although simulations with HIs provide systematically smaller ϕ_c for all the seed sizes. We expect that in the case that HIs would affect the nucleation rate, they would only influence the kinetic aspect of the nucleation process and not the thermodynamic properties. With this regard, we believe that MD + SRD provides lower ϕ_c since finite-size effects are less important in MD + SRD than in MD simulations. In fact, finite-size effects are not only caused by a progressive depletion of colloidal particles in the supersaturated fluid phase which surrounds the growing nucleus, but also by a drop in pressure when the fluid starts to crystallize. The augmented number of particles in the MD + SRD as compared to MD simulations, determined by the explicit presence of SRD point particles in the first method, might reduce the pressure drop and thereby the finite-size effects, thus providing slightly smaller values of ϕ_c.

Finally, we display the extrapolated critical volume fractions in the thermodynamic limit with black points, which are obtained from the finite-size scaling study of Fig. 3(c). The trend is nicely matching with the results obtained in the *NpT* ensemble.

Published under license by AIP Publishing

The seeding approach, in combination with the classical nucleation theory, enables us to compute also the nucleation rate of the system, which is defined as[43]

$$J = \sqrt{|\Delta\mu|/(6\pi k_B T \langle n \rangle)} f^+ \rho_c^{extr} \exp(-\Delta G/k_B T), \quad (6)$$

where $\Delta\mu$ is the chemical potential difference between the fluid and the solid phases at the same temperature and pressure, $\Delta G = |\Delta\mu|\langle n\rangle/2$ is the height of the free energy barrier, and $f^+ = \langle (n(t) - \langle n \rangle)^2 \rangle/(2t)$ is the attachment rate,[6] calculated at the critical density. We calculate the chemical potential of the fluid and solid phases by performing thermodynamic integration of the respective equations of state. The chemical potential of the fluid phase is evaluated at the extrapolated critical densities ρ_c^{extr} for both cases of HIs and no HIs. This is in line with our assumption that the thermodynamic properties of the system should be independent of its kinetic features, hence we expect that the extrapolated critical density should be the same for simulations that exclude and include HIs. The values of ρ_c^{extr} and $\Delta\mu$ are reported in Table II.

In order to compare the dynamical properties of the system for the two cases of HIs included and excluded, we rescale the attachment rate and the nucleation rate by the short-time self-diffusion constant D_0. We estimate D_0 in MD + SRD simulations by performing a linear fit to the mean squared displacement of the colloid particle. We obtain $D_0 = 0.0573 \pm 3 \times 10^{-4} \sigma \sqrt{k_B T/M_c}$. Following Ref. 31, we compute D_0 in MD simulations via the expression $D_0 = 3\sqrt{k_B T/(\pi M_c)}/(8\rho\sigma_{\text{eff}}^2)$, which is obtained from the Chapman–Enskog kinetic theory of gases.[59] The values of $f^+\sigma_{\text{eff}}^2/D_0$ and $J\sigma_{\text{eff}}^5/D_0$ are reported in Table II.

Finally, we plot the values of the nucleation rate obtained with the seeding method as a function of the system volume fraction in Fig. 4, where we also add the previous literature results for comparison. We observe that the seeding method enables us to investigate the nucleation process at very low supersaturation values of the fluid, as we provide the results down to the volume fraction of $\phi = 0.514$ for a seed size of $\langle n \rangle \simeq 630$. The red diamonds and circles represent the results we obtain with simulations that neglect and include HIs in the model, respectively. We see that the two simulation methods provide similar results for all the seed sizes. We also notice that the results corresponding to a seed size of $\langle n \rangle \simeq 215$, at a volume fraction $\phi = 0.524$, fall in a range of volume fractions which was already investigated by other simulation methods, thus directly enabling a comparison with the literature. Our results of the nucleation rate are in very good agreement with the ones obtained via forward flux sampling[27] on hard spheres, thus showing that the seeding approach correctly reproduces the previous results. From this investigation, we conclude that the hydrodynamic interactions do not play a significant role in the kinetic aspects of the nucleation process.

TABLE II. Values of the variables that lead to the computation of the nucleation rate, which are obtained from MD (no HIs) and MD + SRD (HIs) simulations. From the left, we report the seed size $\langle n \rangle$, the extrapolated critical density $\rho_c^{extr}\sigma^3$, the chemical potential difference $\beta|\Delta\mu|$ between the fluid and the solid states at the same temperature and pressure, the attachment rate $f^+\sigma_{\text{eff}}^2/D_0$, and the nucleation rate $J\sigma_{\text{eff}}^5/D_0$. We use the values of $\rho_c^{extr}\sigma^3$ and $\beta|\Delta\mu|$ to calculate the nucleation rate in both cases of "no HIs" and "HIs".

	$\langle n \rangle$	$\rho_c^{extr}\sigma^3$	$\beta\lvert\Delta\mu\rvert$	$f^+\sigma_{\text{eff}}^2/D_0$	$J\sigma_{\text{eff}}^5/D_0$
No HIs	216 ± 27	0.7579	0.3741	1096	3×10^{-17}
	430 ± 26	0.7477	0.2820	3601	1×10^{-25}
	503 ± 41	0.7464	0.2708	3582	5×10^{-29}
	640 ± 17	0.7443	0.2527	2648	9×10^{-35}
HIs	213 ± 21			1033	5×10^{-17}
	430 ± 40	Same as	Same as	2389	6×10^{-26}
	506 ± 58	no HIs	no HIs	2921	3×10^{-29}
	618 ± 50			1576	9×10^{-34}

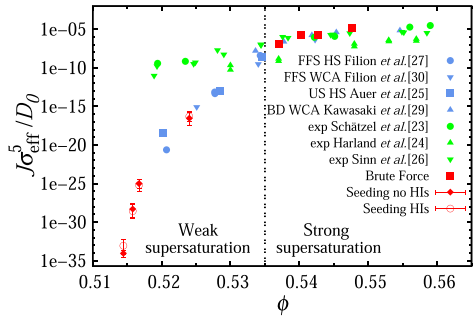

FIG. 4. Nucleation rate $J\sigma_{\text{eff}}^5/D_0$ as a function of the volume fraction ϕ of the system. The red diamonds and circles represent the results we obtain from the seeding method by neglecting and including HIs, respectively. We report our results from brute force simulations with HIs with red squares, the previous numerical results without HIs with blue symbols and the previous experimental results with green symbols.

V. THE STRUCTURE OF THE FLUID

Previous studies showed that the exact local structure of the metastable supersaturated fluid phase, e.g., the presence of FSCs, may affect the nucleation rate of nearly hard-sphere particles.[36,41] This section is dedicated to the analyses of the FSCs in a supersaturated fluid under different physical conditions. In particular, we compute the fraction of defective icosahedral clusters χ, which is defined by the number fraction of particles that belong to a defective icosahedral cluster. We compare the values of χ obtained in a fluid of particles characterized by varying softness of the pair interaction, embedded in various solvent viscosities and affected by a gravitational field at different Péclet numbers. We investigate the fluid at volume fractions $\phi = 0.50$, 0.515, 0.53, and 0.544 and verify that the fraction of crystalline particles is below 1% in all the cases.

A. The role of softer potentials

The softness of a pair interaction is related to the ease by which two particles approach each other closer than their cutoff radius. This feature is reflected by the slope of the interaction potential. The steeper the potential, the harder the pair interaction. In the left panel of Fig. 5(a), we show the interaction potential βU as a function of distance r/σ, for $\beta\varepsilon = 5$, 10, and 40. We observe that the softness of

Published under license by AIP Publishing

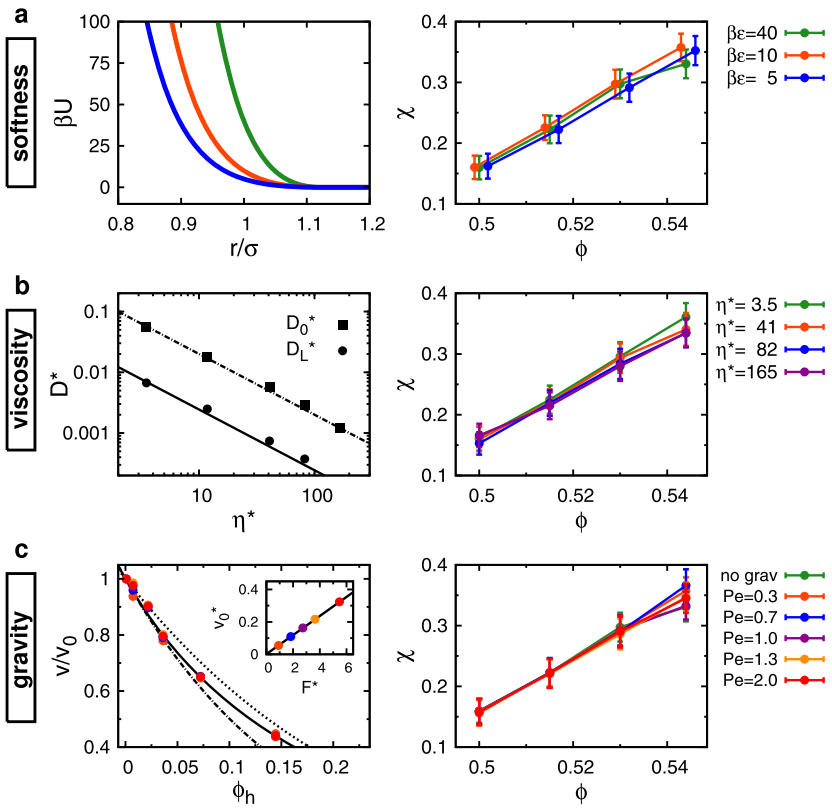

FIG. 5. (a) (Left) Pair potential βU as a function of the distance r/σ, for different softness $\beta\varepsilon$. (Right) Fraction of defective icosahedra χ as a function of the volume fraction ϕ, for different softness $\beta\varepsilon$. (b) (Left) Self-diffusion constant $D^* = D\sqrt{M_c/k_BT}\sigma$ as a function of the solvent viscosity $\eta^* = \eta\sigma^2/\sqrt{M_c k_B T}$. The squares represent the short-time diffusion constant $D_0^* = D_0\sqrt{M_c/k_BT}\sigma$, while the circles represent the long-time diffusion constant $D_L^* = D_L\sqrt{M_c/k_BT}\sigma$, measured on a fluid at a volume fraction $\phi = 0.50$. (Right) Fraction of defective icosahedra χ as a function of the volume fraction ϕ, for different solvent viscosities η^*. (c) (Left) Average terminal velocity v normalized by the Stokes velocity v_0 as a function of the hydrodynamic volume fraction ϕ_h. The dots represent our numerical results, shown with different colors for different Péclet numbers $Pe = v\sigma_{\text{eff}}/2D_0$. The dotted and dashed-dotted lines correspond to two versions of the semiempirical Richardson–Zaki law[60] $v/v_0 = (1-\phi)^a$, with $a = 4.7$ and $a = 6.55$, respectively. The solid line is a theoretical prediction by Hayakawa and Ichiki.[61] The inset shows the reduced Stokes velocity $v_0^* = v_0\sqrt{M_c/k_BT}$ as a function of the reduced drag force $F^* = F\sigma/k_BT$ applied on the colloid. Different colors correspond to different Pe and the solid line is a linear fit to the data points. (Right) Fraction of defective icosahedra as a function of ϕ for different values of Pe.

the potential increases by lowering the repulsion strength $\beta\varepsilon$; therefore, we use these values of $\beta\varepsilon$ to investigate the role of softness in the local structure of the fluid.

In Sec. II, we describe how we prevent the occurrence of spurious depletion effects by choosing the colloid–SRD collision distance $r' = 0.465\sigma$ slightly smaller than the colloid radius 0.5σ. For $\beta\varepsilon = 5$ and 10, the repulsion strength perceived by two colloids at a relative distance of $2r' = 0.93\sigma$ is equal to $\beta U(2r') \simeq 22$ and 44, respectively. These repulsion strengths are large enough to ensure that two colloids will not approach each other at distances closer than $2r'$. In order to verify this statement, we show in Fig. 6 the radial distribution function $g(r)$ of a fluid at a volume fraction of $\phi = 0.515$, for different softness.

We rescale the relative distance r by the effective diameter σ_{eff} of the particle. Note that σ_{eff} depends on the softness of the potential, since we map the freezing volume fraction of each system to the freezing volume fraction of hard spheres, as described in Sec. II. By rescaling the relative distance in this manner, the position of the peaks of the radial distribution functions superimpose on each other. The height of the first peak is slightly larger for harder potentials. This reflects that the distribution increases more steeply for harder potentials at a distance of $r/\sigma \simeq 1$. Since the height of the first peak for $\beta\varepsilon = 5$ and 10 is marginally smaller as compared to $\beta\varepsilon = 40$, we are confident that spurious depletion effects are not present in our model systems, as they would cause a considerable enhancement of the first peak.[47] Moreover, the inset shows a zoom in of the $g(r)$ as a function of the distance r, here rescaled by the bare unit of length σ. In this representation, we can clearly see that $g(r) = 0$ for $r < 0.96\sigma$ for all the softness values considered here, thus demonstrating that two particles never approach each other closer than $2r'$.

The right panel of Fig. 5(a) shows the fraction of defective icosahedra clusters χ as a function of the volume fraction ϕ for different softness, as obtained from MD + SRD simulations. For all

Published under license by AIP Publishing

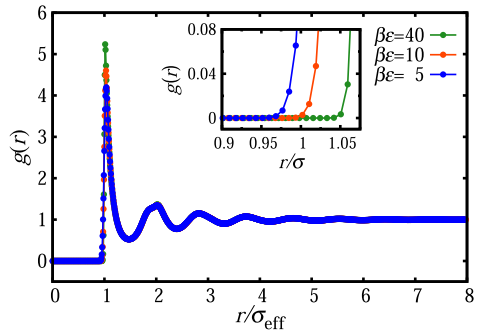

FIG. 6. Radial distribution function $g(r)$ of the fluid at $\phi = 0.515$ for different softness $\beta\varepsilon = 5$, 10, and 40. The distance r is rescaled by the effective diameter σ_{eff}, collapsing all curves on top of each other. The inset shows a zoom in of the $g(r)$ as a function of reduced distance r/σ. The function is zero for $2r' < 0.96\sigma$ for all the softness.

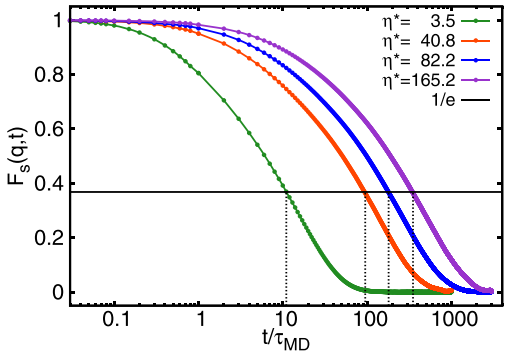

FIG. 7. Self-intermediate scattering function $F_s(q, t)$ as a function of reduced time t/τ_{MD} for different solvent viscosities $\eta^* = \eta\sigma^2/\sqrt{M_c k_B T}$, here represented in different colors. The black lines indicate the value 1/e, which intercepts the functions at the relaxation time τ_r, indicated on the x axis by the dotted lines.

the softness values, we observe that χ increases with increasing the supersaturation of the fluid, as already reported in the literature.[36,41] Different softness values are represented here by different colors. We observe that χ does not show a monotonic trend by varying $\beta\varepsilon$ at fixed ϕ since χ slightly increases as passing from $\beta\varepsilon = 40$ to $\beta\varepsilon = 10$ and slightly decreases as passing from $\beta\varepsilon = 10$ to $\beta\varepsilon = 5$. Moreover, the values of χ at fixed ϕ are consistent within the error bars, especially at lower supersaturation ($\phi \lesssim 0.52$).

The arguments above bring us to conclude that the softness of the interaction potential does not affect the local structure of the fluid within the range of volume fraction investigated in this work. Consequently, this result supports the hypothesis that softness, as represented here, might not influence the rate of nucleation in hard and nearly hard spheres.

B. The role of solvent viscosity

In this section, we simulate four different solvent viscosities $\eta^* = \eta/\eta_0 = 3.5$, 40.8, 82.2, and 165.2. To do so, we increase the number density of SRD particles $5 \leq \gamma a_0^3 \leq 200$. We note that by increasing the viscosity of the system, the simulation time considerably increases due to two independent phenomena. The first one is related to the computational time per time step, which scales linearly with the number of SRD particles. The second one is related to a slowing down of the colloidal particle dynamics, which is caused by a higher friction.

The latter phenomenon is visible in Fig. 7, where we show the self-intermediate scattering function $F_s(q, t)$ as a function of rescaled time t/τ_{MD}, for different solvent viscosities and fixed volume fraction $\phi = 0.515$. This function is defined as $F_s(q,t) = 1/N \sum_{j=1}^{N} \langle \exp\{i\mathbf{q} \cdot [\mathbf{r}_j(0) - \mathbf{r}_j(t)]\}\rangle$, where $\mathbf{q}$ is the wave vector for which we use $q = |\mathbf{q}| = 2\pi/\sigma$, and $\mathbf{r}_j$ is the position vector of particle j. This function describes the positional correlation of a particle with itself over time. It displays high correlation values for short time scales, and a subsequent decay for longer time scales. This decay expresses the progressive decorrelation of the configurations with respect to the initial one, as time elapses.

We define the relaxation time τ_r as the time interval where $F_s(q, \tau_r) = 1/e$. In Fig. 7, we represent the value of $1/e$ with a black line which intercepts each curve at the relaxation time. We indicate τ_r on the x axis by dotted lines in order to guide the eye. The slowing down of the particle dynamics is evident from the increase of τ_r as we enhance the solvent viscosity. For instance, the relaxation time of the red curve is 8.4 times larger than the relaxation time of the green curve. As we further increase the viscosity, the relaxation time becomes 16.2 and 31.2 times larger for the blue and violet curves, respectively.

As is clear from Fig. 7, an increase in viscosity leads to a shift, but crucially not to a qualitative change in the shape of the self-intermediate scattering function. We note that this is a consequence (i) of having sufficiently resolved near-field HIs, which scale linearly with the viscosity, and (ii) of having a sufficiently large separation of time scales between the relaxation of colloidal and fluid velocities,[47] ensuring that on time scales on which the colloids change their configurations, they feel purely viscous effects from the fluid, not influenced by the very short-time ballistic motion of the fluid particles. Note that the shift is proportional to the viscosity for the three highest viscosities in Fig. 7, indicating full separation of time scales. From the lowest viscosity of 3.5 to the next, the shift is almost (but not exactly) proportional to the viscosity, indicating that for the lowest viscosity the time scales are almost (but not quite fully) separated. For each viscosity, we output nearly uncorrelated configurations every multiple of the respective relaxation time such that we perform FSCs analyses on equivalent sets of configurations.

The left panel of Fig. 5(b) shows the colloidal self-diffusion constant as a function of the solvent viscosity. We measure the diffusion constant by performing a linear fit of the mean squared displacement of a particle. The squares represent the short-time diffusion constant D_0, measured in a very dilute system of $\phi \simeq 0.008$, while the circles represent the long-time diffusion constant D_L of a dense fluid at $\phi = 0.50$. In both cases, D scales as $1/\eta$, here visible from the linear scaling in the logarithmic representation of the x and y axes (with a very small deviation for the lowest viscosity, for reasons as discussed above). These results indicate that the hydrodynamics of the system is correctly captured by this simulation method.

Published under license by AIP Publishing

In the right panel of Fig. 5(b), we present the results on the FSCs analysis. We show the number fraction of defective icosahedral clusters χ as a function of volume fraction ϕ for different solvent viscosities. In analogy with the results obtained for different softness of the interaction potential, we observe that χ increases with increasing supersaturation of the fluid, for all the simulated solvent viscosities. Moreover, on a general level, we observe that there is no noticeable effect of the solvent viscosity on the configurational properties of the colloidal fluid. In fact, for each volume fraction, the measurements of χ might slightly vary for different solvent viscosities, but they are consistent with each other within the error bars. For instance, a small difference is found at the highest volume fraction $\phi = 0.544$, since χ decreases by 8% by increasing the solvent viscosity from $\eta/\eta_0 = 3.5$ to $\eta/\eta_0 = 165$. As we lower the supersaturation of the fluid, the value of χ decreases with increasing the solvent viscosity for $\phi = 0.530$ and 0.515, where we measure a difference of 6% and 5%, respectively. On the contrary, χ is larger at $\eta/\eta_0 = 165$ rather than at $\eta/\eta_0 = 3.5$ for $\phi = 0.50$. On the basis of considerations reported in Ref. 36 and explained more deeply in Sec. V C, these differences are too small to cause a sensitive enhancement of the nucleation rate of hard spheres, especially at low supersaturations. Moreover, the opposite trend shown for $\phi = 0.50$ further proves that the solvent viscosity does not affect the local structure of the fluid.

C. The role of gravity

In Fig. 5(c), we present the results obtained for a supersaturated fluid subject to gravity. The left panel shows the average terminal velocity v of the system, normalized by the Stokes velocity v_0, as a function of the hydrodynamic volume fraction ϕ_h. The latter quantity is defined by $\phi_h = 4\pi\rho r_h^3/3$, with the hydrodynamic radius equal to $r_h = 0.363\sigma$. We calculated the hydrodynamic radius via the following equation:

$$r_h = \frac{\zeta_S \zeta_E (\eta_k + 2\eta)}{6\pi\eta(\eta_k + \eta)(\zeta_S + \zeta_E)}, \tag{7}$$

where ζ_S is the Stokes friction and ζ_E the Enskog friction,[47] η is the shear viscosity, and η_k is its kinetic contribution.[47,62] Note that the hydrodynamic radius is somewhat smaller than the colloid–SRD collision radius $r' = 0.465\sigma$, introduced earlier. This is due to an overall smaller friction acting on the colloidal surface which, in turn, affects the strength of the hydrodynamic interactions. We map the hydrodynamics of our model system onto an equivalent physical system by displaying the terminal velocity as a function of the hydrodynamic volume fraction ϕ_h. In fact, the latter quantity encodes the information of the hydrodynamic radius and therefore enables us to quantitatively compare our results with the literature. The values of v/v_0, shown with dots, are in good agreement with both the experimental[63] and the numerical[64] results, the latter performed in the same range of parameters. We observe that collective hydrodynamic effects slow down the settling velocity of the system as the volume fraction is increased. Moreover, the reduction is independent of the Péclet number $Pe = v\sigma_{\text{eff}}/2D_0$, here represented by different colors, in agreement with Ref. 64. The dotted and dashed-dotted lines are two versions of the semi-empirical Richardson–Zaki law[60] $(1-\phi)^a$ with $a = 4.7$ and $a = 6.55$, respectively. The solid line is a theoretical derivation which takes higher-order hydrodynamic interactions into account.[61] The inset displays the reduced Stokes velocity $v_0^* = v_0\sqrt{M_c/k_BT}$ as a function of the reduced external force $F^* = F\sigma/k_BT$ acting on the colloids. The data points perfectly follow a linear trend, shown with a solid black line, which demonstrates that we reproduce a fluid dynamics in the Stokes regime. Moreover, the slope of the linear fit gives an estimate of the diffusion constant $D_0 = 0.0587 \pm 6 \times 10^{-4}\,\sigma\sqrt{k_BT/M_c}$, which results in good agreement with the one measured from the mean squared displacement $D_0 = 0.0573 \pm 3 \times 10^{-4}\,\sigma\sqrt{k_BT/M_c}$ in the absence of gravity.

In the right panel of Fig. 5(c), we report the fraction of defective icosahedra χ as a function of the volume fraction ϕ, for different values of Pe. We observe that χ increases as we increase the supersaturation of the fluid. This trend is in qualitative agreement with the recent experimental results on the same topic.[36] We also find that the amount of χ is rather independent of Pe. In fact, for a fixed volume fraction, the number fraction of defective icosahedra does not significantly change within our error bars. For instance, we obtain that the amount of defective icosahedra at $Pe = 2$ differs by 3% from the value obtained in the absence of gravity, whereas the relative error of the measurements is about 10%. However, the irrelevance of gravitational effects on the amount of FSCs is surprisingly in contrast with the experimental results mentioned above, where they find a reduction of defective icosahedra between 34% and 24% in the range of $0.50 < \phi < 0.544$, for $Pe = 1.5$ as compared to the density matched case.

The cause of this divergence between experiments and simulations is not clear yet. For what concerns our numerical results, we are confident that the SRD method accurately captures the hydrodynamics of the system. In fact, we demonstrate this by nicely reproducing the decay of the terminal velocity of the system as a function of the volume fraction. Yet, we note that the hydrodynamic radius is slightly smaller than the radius of the colloid. This implies that the magnitude of hydrodynamic interactions, which scales linearly with the hydrodynamic radius, is somewhat smaller in our model system as compared to an actual system. Despite this, we believe that the weakening of hydrodynamic interactions is not so relevant to justify the discrepancy between simulations and experiments. A more rigorous matching between the experimental and simulation results would require further quantitative analyses on the differences inherently present in these two systems. We leave this additional investigation for future research, as we believe it is out of the scope of the current work.

VI. CONCLUSIONS

We performed MD + SRD simulations of nearly hard spheres in order to investigate whether hydrodynamic interactions may enhance the crystal nucleation rate, and may bridge the long-standing discrepancy between the numerical and experimental results. To do so, we addressed the problem from different angles and employed several simulation methods. In all the cases investigated, we found that HIs do not influence the crystal nucleation rate either directly or indirectly, thereby leaving the problem unresolved.

In the first part of this work, we computed the nucleation rate in a wide range of fluid volume fractions by means of two

Published under license by AIP Publishing

simulation methods. At high supersaturations, we employed brute force MD + SRD simulations to directly observe the spontaneously forming crystal nuclei. We computed the nucleation rate and showed that our results agree well with the previously reported values, thereby validating the use of this simulation technique in this context.

At low fluid supersaturations, we employed the seeding approach method and performed MD simulations with and without HIs. We compared the nucleation rates obtained in these two cases and found a remarkably good agreement between them. Therefore, the presence of hydrodynamic interactions in the system does not influence the crystal nucleation rate, in direct contrast with what is hypothesized in previous studies that did not account for HIs.[27,29–32,36,43] The obtained nucleation rates follow the trend of earlier numerical results, thus leaving open the issue of the discrepancy between experiments and simulations.[6,23–27,29,30,36]

Thus, our result that the presence of hydrodynamic interactions does not influence the crystal nucleation rate is in contrast to the work of Radu and Schilling[34] that demonstrated that the nucleation rate is enhanced at high viscosities. The difference is caused by the way the hydrodynamic interactions are implemented.[65]

First, the interactions between the colloids and the SRD particles are assumed to be ideal in Refs. 34 and 65, whereas in our case, we implemented excluded volume interactions between the colloids and the SRD particles. The near-field hydrodynamics, which can only be captured by taking into account the excluded volume between the colloids and the SRD fluid, is hence not resolved in Refs. 34 and 65. To be more specific, this means that the lubrication forces which scale linearly with viscosity, the near-field hydrodynamic fluid flow field around the surface of the colloids, and the Brownian motion due to the collisions between the colloids and the SRD particles are not captured in the work of Radu and Schilling.[34,65] We expect the lubrication forces to be dominant at the high packing fractions that are required to study crystal nucleation.

Second, the mass of the colloids M is set equal to the mass of the SRD particles m, i.e., $M = m$ in Refs. 34 and 65, whereas in the present work, we made sure that the colloid mass M is much larger than the mass of the SRD particles, i.e., $M \gg m$. Hence, there is no clear separation of time scales between the motion of the colloids and the motion of the fluid in Refs. 34 and 65, and the colloids behave more like another solvent particle than a suspended colloidal particle.

Third, in the study of Refs. 34 and 65, the viscosity is altered by changing the SRD collision interval, whereas in our case, the viscosity is tuned by changing the number density of SRD particles so that the kinematic viscosity (viscosity divided by the solvent number density) is kept constant. As the kinematic viscosity increases largely in Refs. 34 and 65 with viscosity, the diffusion coefficient of the colloids scales non-linearly upon changing viscosity, indicating that the hydrodynamics is not fully captured by this method. Moreover, at low viscosity, the collision time is smaller than the collision time of the SRD particles, and thus, the motion of the colloids is not fully controlled by the solvent viscosity, but rather by inertia or ballistic effects.

In the second part of this work, inspired by the hypothesis that FSCs might compete against nucleation already at lower fluid supersaturation than the glass transition, we further investigated the properties of the system from this perspective. We simulated a supersaturated fluid of nearly hard spheres with HIs in a volume fraction range of $0.50 < \phi < 0.544$ and computed the fraction of defective icosahedra χ in the system under different physical conditions.

First, we studied the role of the pair interaction softness by simulating three different temperatures $\beta\varepsilon = 40$, 10, and 5. We compared the values of χ in the three cases and found good agreement among them, especially at lower supersaturation values. With this regard, we conclude that the interaction softness does not influence the local structure of the fluid, especially the fraction of FSCs.

Second, we explored different values of the solvent viscosity, which was varied in the range of $3 < \eta/\eta_0 < 165$. Because of the clear separation of time scales for relaxation of the colloidal and fluid velocities, the colloidal dynamics was found to slow down linearly with increasing viscosity, as expected. We found that χ slightly decreases with increasing solvent viscosity at high supersaturation, although the decrement is very small (~6% for $\phi = 0.530$) and should definitely not lead to a significant difference in the nucleation rate. In fact, in a recent study[36] on the same topic, it was shown that a difference of χ of about 30% is still not sufficient to recover the experimental nucleation rates. At low supersaturations, we found hardly any effect of viscosity on χ, and hence, the discrepancy between experiments and simulations remains unexplained.

Finally, we studied the system under gravity, for values of $Pe < 2$. Similarly to what we obtained by varying other system properties, the local structure of the fluid is insensitive to different sedimentation rates. This result is surprising as it shows a net contrast with the recent work of Wood *et al.*,[36] where a settling fluid at $Pe = 1.5$ displays 30% less defective icosahedra as compared to the non-settling fluid.

To conclude, we consistently find a substantial irrelevance of the hydrodynamic interactions on the nucleation rate and the local structure of the supersaturated fluid. Despite the fact that our findings do not explain the enduring discrepancy between experiments and simulations on the nucleation rate, they have disproved the hypothesis, coming from previous numerical studies, that HIs are the missing ingredient to recover the experimental nucleation rates. Perhaps HIs are important, but then in combination with another physical mechanism not explored in our work. Furthermore, we opened new interesting research directions to be investigated, e.g., a joint experimental and numerical study on the properties of the fluid under gravity.

After our submission, we became aware of another recent simulation study[66] that investigated the effect of hydrodynamic interactions by implementing the Fluid Particle Dynamics method on the kinetics of nucleation and growth of nearly hard spheres. This study shows agreement with our findings that hydrodynamic interactions do not seem to affect the nucleation rates when scaled by the long-time diffusion coefficient of the colloids.

AUTHOR'S CONTRIBUTIONS

G.F. performed computer simulations and analyses to study the nucleation rate of the system, via brute force simulations and the seeding approach method, and the local structure of the supersaturated fluid under gravity by varying the softness of pair interactions and the solvent viscosity.

Published under license by AIP Publishing

G.M.C. computed the particle effective diameter for $\beta\varepsilon = 10$ and 5 via free energy calculations.

ACKNOWLEDGMENTS

This work was supported by The Netherlands Center for Multiscale Catalytic Energy Conversion (MCEC), a NWO Gravitation program funded by the Ministry of Education, Culture and Science of the government of The Netherlands. G.F. gratefully thanks L. Filion for providing the values of the chemical potential in the fluid and crystal phases. G.F. is grateful to T. Dasgupta for providing the code to compute the intermediate scattering function. G.F. thanks Joost de Graaf, S. Paliwal, and G. Avvisati for fruitful discussions.

REFERENCES

[1] W. W. Wood and J. D. Jacobson, J. Chem. Phys. **27**, 1207 (1957).
[2] B. J. Alder and T. E. Wainwright, J. Chem. Phys. **27**, 1208 (1957).
[3] A. Vrij, J. W. Jansen, J. K. Dhont, C. Pathmamanoharan, M. M. Kops-Werkhoven, and H. M. Fijnaut, Faraday Discuss. Chem. Soc. **76**, 19 (1983).
[4] P. N. Pusey and W. van Megen, Nature **320**, 340 (1986).
[5] V. J. Anderson and H. N. W. Lekkerkerker, Nature **416**, 811 (2002).
[6] S. Auer and D. Frenkel, Adv. Polym. Sci. **173**, 149 (2005).
[7] R. P. Sear, J. Phys.: Condens. Matter **19**, 033101 (2007).
[8] U. Gasser, J. Phys.: Condens. Matter **21**, 203101 (2009).
[9] K. F. Kelton and A. L. Greer, *Nucleation in Condensed Matter* (Pergamon, New York, 2010), Vol. 15, p. 726.
[10] D. M. Herlach, T. Palberg, I. Klassen, S. Klein, and R. Kobold, J. Chem. Phys. **145**, 211703 (2016); arXiv:1605.03511.
[11] J. Frenkel, J. Chem. Phys. **7**, 538 (1939).
[12] D. Erdemir, A. Y. Lee, and A. S. Myerson, Acc. Chem. Res. **42**, 621 (2009).
[13] R. P. Sear, Int. Mater. Rev. **57**, 328 (2012).
[14] S. Karthika, T. K. Radhakrishnan, and P. Kalaichelvi, Cryst. Growth Des. **16**, 6663 (2016).
[15] J. Russo and H. Tanaka, MRS Bull. **41**, 369 (2016); arXiv:1611.07165.
[16] M. Volmer and A. Weber, Z. Phys. Chem. **119U**, 277 (2017).
[17] R. Becker and W. Döring, Ann. Phys. **416**, 719 (1935).
[18] T. Schilling, H. J. Schöpe, M. Oettel, G. Opletal, and I. Snook, Phys. Rev. Lett. **105**, 025701 (2010); arXiv:1003.2552.
[19] J. T. Berryman, M. Anwar, S. Dorosz, and T. Schilling, J. Chem. Phys. **145**, 211901 (2016); arXiv:1503.07732.
[20] H. Tanaka, J. Stat. Mech.: Theor. Exp. **2010**, P12001.
[21] H. Tanaka, T. Kawasaki, H. Shintani, and K. Watanabe, Nat. Mater. **9**, 324 (2010).
[22] J. Russo and H. Tanaka, Sci. Rep. **2**, 505 (2012); arXiv:1109.0107.
[23] K. Schätzel and B. J. Ackerson, Phys. Rev. E **48**, 3766 (1993).
[24] J. L. Harland and W. van Megen, Phys. Rev. E **55**, 3054 (1997).
[25] S. Auer and D. Frenkel, Nature **409**, 1020 (2001).
[26] C. Sinn, A. Heymann, A. Stipp, and T. Palberg, Prog. Colloid Polym. Sci. **118**, 266 (2001).
[27] L. Filion, M. Hermes, R. Ni, and M. Dijkstra, J. Chem. Phys. **133**, 244115 (2010).
[28] C. P. Royall, W. C. Poon, and E. R. Weeks, Soft Matter **9**, 17 (2013).
[29] T. Kawasaki and H. Tanaka, Proc. Natl. Acad. Sci. U. S. A. **107**, 14036 (2010).
[30] L. Filion, R. Ni, D. Frenkel, and M. Dijkstra, J. Chem. Phys. **134**, 134901 (2011).
[31] D. Richard and T. Speck, J. Chem. Phys. **148**, 124110 (2018); arXiv:1803.05218.
[32] D. Richard and T. Speck, J. Chem. Phys. **148**, 224102 (2018); arXiv:1805.05689.
[33] J. D. Weeks, D. Chandler, and H. C. Andersen, J. Chem. Phys. **54**, 5237 (1971); arXiv:NIHMS150003.
[34] M. Radu and T. Schilling, EPL (Europhys. Lett.) **105**, 26001 (2014); arXiv:1301.5592.
[35] D. Roehm, S. Kesselheim, and A. Arnold, Soft Matter **10**, 5503 (2014); arXiv:1304.4158v1.
[36] N. Wood, J. Russo, F. Turci, and C. P. Royall, J. Chem. Phys. **149**, 204506 (2018); arXiv:1809.03825v1.
[37] S. Ketzetzi, J. Russo, and D. Bonn, J. Chem. Phys. **148**, 064901 (2018).
[38] J. Russo, A. C. Maggs, D. Bonn, and H. Tanaka, Soft Matter **9**, 7369 (2013); arXiv:1307.0658.
[39] F. C. Frank, Proc. R. Soc. London, Ser. A **215**, 43 (1952).
[40] J. L. Finney, Proc. R. Soc. A **319**, 495 (1970).
[41] J. Taffs and C. P. Royall, Nat. Commun. **7**, 13225 (2016).
[42] J. R. Espinosa, C. Vega, C. Valeriani, and E. Sanz, J. Chem. Phys. **142**, 194709 (2015).
[43] J. R. Espinosa, C. Vega, C. Valeriani, and E. Sanz, J. Chem. Phys. **144**, 034501 (2016).
[44] S. Plimpton, J. Comput. Phys. **117**, 1 (1995); arXiv:nag.2347 [10.1002].
[45] M. K. Petersen, J. B. Lechman, S. J. Plimpton, G. S. Grest, P. J. in 't Veld, and P. R. Schunk, J. Chem. Phys. **132**, 174106 (2010).
[46] A. Malevanets and R. Kapral, J. Chem. Phys. **110**, 8605 (1999).
[47] J. T. Padding and A. A. Louis, Phys. Rev. E **74**, 031402 (2006); arXiv:0603391 [cond-mat].
[48] M. Hecht, J. Harting, T. Ihle, and H. J. Herrmann, Phys. Rev. E **72**, 011408 (2005); arXiv:0502028 [cond-mat].
[49] D. S. Bolintineanu, J. B. Lechman, S. J. Plimpton, and G. S. Grest, Phys. Rev. E **86**, 066703 (2012).
[50] E. Tüzel, M. Strauss, T. Ihle, and D. M. Kroll, Phys. Rev. E **68**, 15 (2003); arXiv:0304599 [cond-mat].
[51] M. Theers, E. Westphal, K. Qi, R. G. Winkler, and G. Gompper, Soft Matter **14**, 8590 (2018).
[52] A. Ahmed and R. J. Sadus, Phys. Rev. E **80**, 061101 (2009).
[53] D. Frenkel and B. Smit, *Understanding Molecular Simulation: From Algorithms to Applications* (Elsevier, 2001), Vol. 1.
[54] D. Frenkel and A. J. C. Ladd, J. Chem. Phys. **81**, 3188 (1984).
[55] J. M. Polson, E. Trizac, S. Pronk, and D. Frenkel, J. Chem. Phys. **112**, 5339 (2000).
[56] P. J. Steinhardt, D. R. Nelson, and M. Ronchetti, Phys. Rev. B **28**, 784 (1983).
[57] P. R. ten Wolde, M. J. Ruiz-Montero, and D. Frenkel, Faraday Discuss. **104**, 93 (1996).
[58] A. Malins, S. R. Williams, J. Eggers, and C. P. Royall, J. Chem. Phys. **139**, 234505 (2013).
[59] S. Chapman, T. G. Cowling, and D. Burnett, *The Mathematical Theory of Non-uniform Gases* (Cambridge University Press, 1970).
[60] M. Robins and A. Fillery-Travis, J. Chem. Tech. Biotechnol. **54**, 201 (1992).
[61] H. Hayakawa and K. Ichiki, Phys. Rev. E **51**, R3815 (1995).
[62] M. Theers, E. Westphal, G. Gompper, and R. G. Winkler, Phys. Rev. E **93**, 032604 (2016).
[63] R. Piazza, Rep. Prog. Phys. **77**, 056602 (2014).
[64] J. T. Padding and A. A. Louis, Phys. Rev. Lett. **93**, 220601 (2004); arXiv:0409133 [cond-mat].
[65] M. Radu, "Crystallization in hard sphere systems," Ph.D. thesis, Université du Luxembourg, 2013.
[66] M. Tateno, T. Yanagishima, J. Russo, and H. Tanaka, Phys. Rev. Lett. **123**, 258002 (2019).

Published under license by AIP Publishing